POLITECNICO DI TORINO
Repository ISTITUZIONALE

Modelling the efficacy of CAR-CIK cell immunotherapy targeting MET-expressing mesothelioma cells

Original
Modelling the efficacy of CAR-CIK cell immunotherapy targeting MET-expressing mesothelioma cells / Padovano, F., Lombardi, A.M., Novello, S., Lorenzi, T., Vigna, E., Leschiera, E., Villa, C.. - In: SCIENTIFIC REPORTS. - ISSN 2045-2322. - (2026). [10.1038/s41598-026-64219-y]

Availability:
This version is available at: 11583/3017688 since: 2026-11-09T08:19:45Z

Publisher:
Springer Nature

Published
DOI:10.1038/s41598-026-64219-y

Terms of use:

This article is made available under terms and conditions as specified in the corresponding bibliographic description in the repository

Publisher copyright

(Article begins on next page)

29 November 2026

ARTICLE | Article in Press

Modelling the efficacy of CAR-CIK cell immunotherapy targeting MET-expressing mesothelioma cells

Federica Padovano · Andrea Maria Lombardi · Silvia Novello · Tommaso Lorenzi · Elisa Vigna · Emma Leschiera · Chiara Villa

Received: 15 April 2026 / Accepted: 23 July 2026
© The Author(s) 2026

Abstract

Malignant pleural mesothelioma (MPM) is an aggressive tumour associated with poor prognosis and limited treatment options, motivating the investigation of novel therapeutic approaches. Among these, chimeric antigen receptor (CAR)–based adoptive cell therapy has attracted considerable interest given its potential to achieve durable clinical responses. In this paper, we combine experimental and mathematical approaches to investigate the efficacy of a CAR-based immunotherapy using cytokine-induced killer (CIK) cells engineered with a MET-specific receptor targeting MET-expressing tumour cells. In vitro data from diverse MPM cell lines and CIK preparations are used to develop and calibrate a mathematical model describing the interaction dynamics between tumour cells, structured by their MET expression level, and CIK cells. The model successfully reproduces experimental observations and is used to predict treatment efficacy under previously untested conditions, which are validated with new data from MPM primary cell lines, supporting the robustness of the mathematical framework. Our results elucidate the interplay between three key factors positively impacting treatment efficacy: the initial immune-to-tumour cell ratio, the percentage of CAR-MET-expressing CIK cells generated upon engineering, and the MET expression level of tumour cells. Together, these findings provide a quantitative basis for assessing CAR-CIK therapy effectiveness, which supports clinical decision making.

Introduction

Biological context

The natural immune system can target malignant cells, which can be recognised as non-self and thus eliminated. However, tumours frequently disrupt effective immune responses. Cancer immunotherapy seeks to leverage the specificity of the natural immune response and aims to increase its effectiveness through the application of advances in cellular and molecular immunology[1].

This Article in Press is shared early to give you faster access to new research. It is citable and carries a permanent DOI. The final edited version will replace it automatically.

These authors contributed equally: Federica Padovano and Andrea Maria Lombardi.

These authors jointly supervised this work: Emma Leschiera and Chiara Villa.

https://doi.org/10.1038/s41598-026-64219-y

Published online: 01 October 2026

Among the immunotherapeutic approaches developed to reinforce antitumour immune responses, adoptive cell therapy (ACT) has gained increasing attention over the past three decades due to its potential to achieve durable clinical responses[2]. ACT encompasses strategies employing T lymphocytes or other immune effector cells that are expanded, modified, or genetically engineered *ex vivo* to enhance antitumour activity prior to reinfusion into the patient[3,4]. Within this landscape, chimeric antigen receptor (CAR)-based approaches represent one of the most promising ACT strategies. CARs are synthetic receptors that enable T lymphocytes to directly recognise tumour-associated antigens independently of major histocompatibility complex (MHC) presentation[5], which is normally required for T-cell recognition. Currently, CAR-T therapies are the standard of care for treating a subset of hematological malignancies[6]. On the contrary, solid tumours, characterised by high complexity, represent a challenge for the successful application of CAR-based immunotherapy[7]. Indeed, therapeutic outcomes remain highly variable and depend on complex interactions among engineered immune cells, tumour burden, antigen expression, microenvironmental factors, and treatment parameters, which are difficult to dissect experimentally[4,8]. In this frame, tools to refine and predict the efficacy of CAR-based immunotherapies are strongly sought.

Here, we consider Malignant Pleural Mesothelioma (MPM), a highly aggressive tumour characterised by poor prognosis, limited therapeutic options, and the absence of curative treatments[9,10]. We use MPM as a model to study the response to a CAR-immunotherapy based on the employment of unconventional immune effectors with a mixed natural killer (NK)-T phenotype, namely cytokine-induced killer (CIK) cells. CIK cells display high *in vitro* proliferative capacity, efficient tumour trafficking, and potent MHC-unrestricted cytotoxic activity mediated by the NKG2D receptor and have demonstrated a favorable safety profile across multiple tumour types[11]. Within this framework, CIK cells have been engineered to express a CAR recognising the MET receptor exposed on the surface of MPM cells. MET is a transmembrane tyrosine kinase receptor involved in tumour initiation and progression[12] and is frequently overexpressed in MPM, where it correlates with poor prognosis[13], while is absent or very low in adult tissues, in physiological conditions.

CAR-MET.CIK and MPM cells are here exploited as a paradigm for a quantitative analysis of cancer-immune cell dynamics, through the development and the validation of a mathematical model suitable to support the rational design and optimization of CAR-ACT strategies.

Mathematical modelling framework

Mathematical modelling represents a powerful framework for investigating biological systems and has gained increasing relevance in oncology, where it is used to characterise, quantify, and predict the complex mechanisms driving cancer evolution[14]. Numerous studies in the literature have focused on modelling tumour-immune cell interactions[15–18]. Commonly formulated as predator-prey systems of ordinary differential equations (ODEs), these models can capture the key mechanisms influencing the tumour immune response, including immune cell expansion and differentiation, immune cell infiltration, tumour-induced immunosuppression, as well as tumour adaptation and resistance to immune-mediated cytotoxicity.

More recently, the emergence of CAR-T cell therapies has motivated the development of dedicated mathematical models to achieve a precise understanding of treatment dynamics and therapeutic outcomes[19–22]. These models are particularly useful for quantifying CAR-T cytotoxic efficacy, whether administered alone or in combination with other therapies[23], and for assessing the influence of factors such as antigen heterogeneity[24,25], CAR-T cell kinetics[26], and memory-effector T-cell differentiation[27].

Since immune cell killing efficacy strongly depends on tumour associated antigen expression, it is particularly relevant to structure tumour cells by the level of expression of the T-cell receptor-specific antigen, as done in[28]. Models of this type, commonly formulated as partial integro-differential equations (PIDEs) describing the dynamics of the cell phenotypic distribution[29,30], explicitly account for intra-population heterogeneity and protein expression-modulated processes. In our context, this framework enables us to capture heterogeneity in MET expression level within the MPM cell population, which directly influences the cytotoxic activity of CAR-MET. CIK cells.

Several of these modelling approaches have been integrated with experimental or clinical data[24,31–33], with the ultimate goal of supporting biologists and clinicians in identifying critical scenarios for empirical testing, and in designing optimised and personalised therapeutic strategies.

Contents and structure of the article

We propose a synergistic experimental and mathematical modelling approach, to evaluate the efficacy of CAR-MET.CIK cell immunotherapy on MPM cells. Data from *in vitro* experiments are used to inform the mathematical model, which comprises a PIDE for the dynamics of a population of tumour cells structured by their level of MET expression, coupled with ODEs describing the dynamics of two CIK cell subpopulations, namely CAR-MET-expressing cells and CAR-MET-negative control cells. These model features enable us to assess the impact on immunotherapy efficacy of three baseline metrics: the MET expression level of tumour cells, the percentage of CAR-MET-expressing CIK cells generated upon engineering, and the immune-to-tumour cell initial ratio.

Experimental data are first employed in a systematic model selection procedure based on the well-established Akaike Information Criteria (AIC)[34], and then used to calibrate the selected model with a Bayesian inference approach. This allows us to estimate posterior parameter distributions encoding variability across cell lines, and thus account for such variability in model predictions which go beyond previously tested experimental scenarios. Finally, model predictions are validated against new MPM primary cell data.

The paper is organized as follows. Section "Materials and methods" presents the methodology, covering the *in vitro* assays and associated data collection and processing procedures, the mathematical model assumptions and equations, and the model selection and calibration methodology. Section "Results" reports on the results of *in vitro* assays, model selection and calibration, along with the model-based predictions and their validation. Section "Discussion" includes a discussion on the strengths and limitations of the model in relation to its performance and translational relevance. Finally, "Conclusions" concludes the paper.

Materials and methods

In vitro experimental data

Cells

MERO-25, and SPC-212 were from the European Collection of Authenticated Cell Cultures (ECACC). MSTO-211H, NCI-H2052, NCI-H28 were from the American Type Culture Collection (ATCC). Cell lines were cultured according to the manufacturer's instructions. M-45PE, M-89, and SL-188 primary cells derived from human pleural mesothelioma sample have been described in Anobile et al.[35]. After stabilization, primary cell lines were cultured in RPMI-1640 medium, 10% Fetal Bovine Serum (FBS), 1% L-glutamine, 1% penicillin, and 1% streptomycin (Gibco™ Thermofisher Scientific). Cell cultures were routinely checked for Mycoplasma SPP contamination (MycoStrp™ InvivoGen).

Isolation, activation, transduction, and expansion of CAR-MET.CIKs

CIK cells have been derived from human healthy donor or patient samples, collected following the provision of written informed consent. The experiments were conducted in accordance with the principles of the Declaration of Helsinki, the International Conference on Harmonisation guidelines, Good Clinical Practice, and the General Data Protection Regulation (GDPR). Buffy coats from healthy donors (residual blood-derived materials) were obtained from the Blood Bank and Immunohematology Laboratory of the AOU Città della Salute e della Scienza di Torino, under the formal agreement no. 993/2023 between this Institution and the Department of Oncology of

the University of Torino. Cancer patient blood samples were collected following the approval by the Comitato Etico Territoriale Interaziendale, AOU Città della Salute e della Scienza di Torino, reference no. 125/2022 (last version of the protocol approved on 05/02/2025). Peripheral Blood Mononuclear Cells (PBMC) isolated from blood samples by density gradient centrifugation (Lymphosep, Aurogene srl) were seeded on day 0 in cell culture flasks at a concentration of 2×10^6 cells/mL with IFNγ (Miltenyi Biotec; 1000 U/mL) in RPMI-1640 medium, 10% FBS (Value FBS, Thermofisher Scientific), 1% L-glutamine, 1% penicillin, and 1% streptomycin. After 24 hours of culture, PBMC were activated by Anti-Biotin MACSi Bead Particles loaded with anti-CD2, -CD3, and -CD28 mAbs (Miltenyi Biotec) and human interleukin-2 (human recombinant IL-2 IS 300, U/mL, Miltenyi Biotec). To generate CAR-MET.CIKs, on day +2, cells were transduced with CAR-MET/eGFP Bidirectional lentiviral vector (LV)[36]. LV have been prepared and validated as described in Chiriaco et al.[36]. For transduction, cells were plated in a 24 well plate at a density of 10^6 cells/well in 300 μL of medium with IL-2 (500 U/mL) and LV at MOI 10. Not transduced (NTD) CIKs were used as a paired control. Both CAR-MET.CIK and NTD.CIK were expanded over 3-5 weeks. At day 12-15 CIKs phenotype maturation was assessed as described in Leuci et al.[37]. Every 2-3 days fresh medium with IL-2 (300 U/mL) was added to maintain the cell density as 1.5×10^6 cells/mL. Different CIK preparations were used, denoted A, B, C and D in the following, corresponding to CAR.CIKs transduced at the levels 15%, 27%, 42% and 24%, respectively. Three additional CIK preparations were used for model validation, denoted E (20%), F (23%) and G (33%).

Flow cytometry analysis

CAR expression on CIK ($CAR_{\%}$) was evaluated at day 12-14 by Alexa Fluor[IEq not found] 647 AffiniPure F(ab')$_2$ Fragment Goat Anti-Human IgG (H+L) antibody, binding the CAR-MET hinge region or by Alexa Fluor[IEq not found] 647 AffiniPure F(ab')$_2$ Fragment Goat Anti-Mouse IgG, F(ab')$_2$ fragment specific (Jackson Immuno Research). MET expression on tumour cells was assessed by Human HGFR/c-MET APC-conjugated Antibody, clone #95106 (R&D System). For NKG2D ligands expression on tumor cells, were analised by: Mouse anti-Human MIC A/B PE-conjugated Antibody, clone 6D4 (BD Bioscience); Mouse anti-Human ULBP 2-5-6 APC-conjugated, clone #165903 (R&D System); Mouse anti-Human ULBP 3 PE-conjugated, clone #166510 (R&D System); Mouse anti-Human ULBP 1 Alexa-Fluor488-Conjugated, #170818 (R&D System). Labeled cells were analysed on BD FACSCelesta™ Cell Analyzer (BD Biosciences, USA). Gate criteria were set to unstained Ab controls. The fraction of CAR-MET ($CAR_{\%}$) or MET positive cells ($MET_{\%}$), and the Mean Intensity of Fluorescence (MFI), indicative of MET receptor density on the cell surface, has been evaluated using Kaluza Software (Beckman Coulter, Inc.).

Cell growth assay

MPM cells were seeded 2000/well in a 96 well plate in complete medium. Cell viability was determined after 8 hours (day0), and every 24 hours for 4 consecutive days by CellTiter-Glo luminescent cell viability assay (Promega Corp.), according to the manufacturer's instructions. Chemiluminescence was detected with the multimode plate reader EnSpire (Perkin Elmer Inc). For CIK, cells were counted with Trypan blue (Gibco™ Thermofisher Scientific) to evaluate only viable cells. Fold expansion was evaluated starting from day +3 of the expansion procedure (corresponding to time 0) every 2/3 days for two weeks.

In vitro cytotoxicity assays

Target cells were labeled with the vital dye PKH26 (Sigma-Aldrich) following the manufacturer's protocols. Target cells (10.000/well in a 48 well plate) were co-cultured in RPMI-1640 medium enriched with 10%FCS and IL-2 (300 U/mL) with effector cells at various effector-to-target (E:T) ratios (5 : 1, 2.5 : 1, 1 : 1, 1 : 2 and 1 : 4) for 48 hours (NCI-H28, MSTO-211H, SPC-212, NCI-H2052, and MERO-25) or 72 hours (M-45PE, M-89, and

SL-188). The cytotoxic effect was quantified by measuring the percentage of PKH26+/DAPI- tumour cells by cytofluorimeter analysis on BD FACSCelesta™ Cell Analyzer (BD Biosciences, USA). To evaluate spontaneous cell death, target cells were cultured in the same conditions without adding CIKs. The percentage of tumour-specific killing, denoted as TSK, for each E:T ratio was calculated using the following formula[37]:

$$\mathrm{TSK} = \frac{(\text{experimental mortality} - \text{spontaneous mortality})}{(100 - \text{spontaneous mortality})} \times 100 \tag{1}$$

where *experimental mortality* is the percentage of cells scored as dead in a sample, including those that died as a consequence of a treatment and those that died naturally, and *spontaneous mortality* is the percentage of cells that died naturally in the absence of treatment (Fig. 1).

Mathematical model

We develop a mathematical model that describes the interaction dynamics between a population of tumour cells, structured by the level of MET expression, and both NTD.CIK and CAR-MET.CIK lymphocytes.

Model variables

We introduce the tumour cell population density function $\hat{n}(t,y) \geq 0$, which represents the number of tumour cells with level of MET expression $y \in [0, y_H]$ at time $t \in \mathbb{R}_{>0}$. We assume that there exists a MET level $y_H \in \mathbb{R}_{>0}$, endowing cells with the highest expression level of MET. Based on the MET expression distribution data we fix $y_H = 4 \times 10^4$. We then introduce the change of variable $x := y/y_H$, so that the rescaled MET-related phenotypic trait $x = 1$ corresponds to the maximum MET-expression level $y = y_H$. Under this change of variable, we hereon consider the rescaled tumour cell population density function $n(t,x) = y_H\, \hat{n}(t,y) \geq 0$, and compute the total tumour cell number as

$$\rho_n(t) := \int_0^1 n(t,x)\,\mathrm{d}x\,. \tag{2}$$

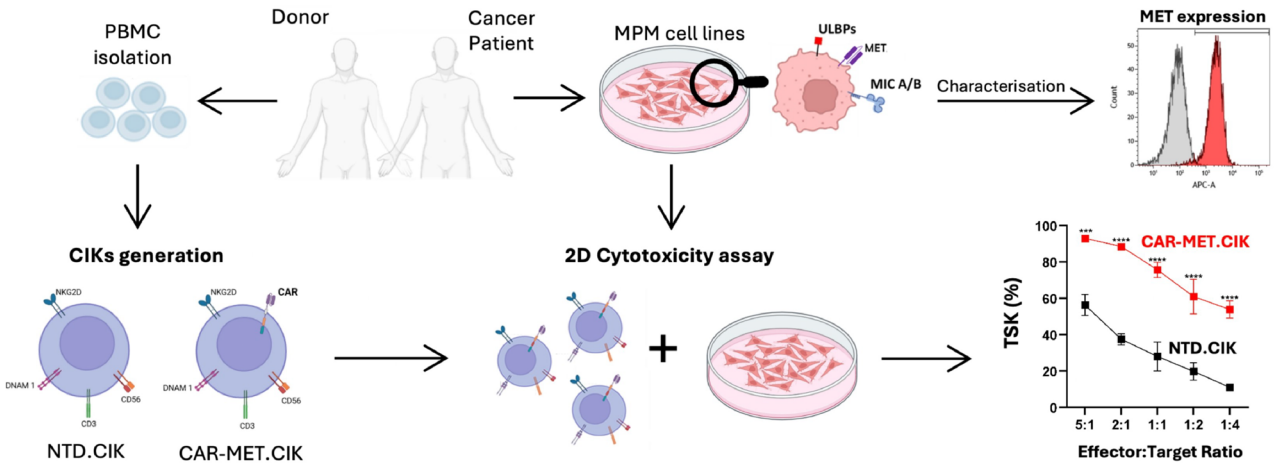

Figure 1 Graphical scheme of the experimental setup. CIK cells were generated from PBMCs isolated from healthy donors, and genetically engineered to express a CAR targeting the MET receptor expressed on the surface of *ex vivo* MPM cells. NTD.CIK and CAR-MET.CIK cells respectively denote the not-transduced and CAR-expressing CIK cells following lentiviral vector transduction. NTD.CIK cells were used as controls for the assessment of CAR-MET.CIK cytotoxicity – cf. black vs red TSK curves, TSK defined in (1). Created with Biorender.com, accessed on November 2025 with a University of Turin- Department of Oncology license.

We also introduce the functions $c_1(t) \geq 0$ and $c_2(t) \geq 0$, which model, respectively, the number of CAR-MET.CIK and NTD.CIK cells at time t, and denote by $c(t) = c_1(t) + c_2(t) \geq 0$ the corresponding total number of CIK cells in the system. We denote by $N_N(t) \geq 0$ and $N_C(t) \geq 0$ the number of tumour cells that died at time t due to natural causes and killed by CIK cells, respectively. Finally, to compare model outputs to the experimental TSK defined in Eq. (1), we introduce the numerical TSK, f_{TSK}, which is defined in Sect. 2.2.

Model equations and hypotheses tested

The dynamics of the rescaled tumour cell density, $n(t, x)$, coupled with the dynamics of CAR-MET.CIK, $c_1(t)$, and NTD.CIK, $c_2(t)$, cells is governed by the following system of equations

$$\begin{cases} \partial_t n = (\Phi_n(\rho_n) - \Gamma(c, \rho_n) - k(x)\Psi(c_1, \rho_n))\, n, \\ N_N' = \mu_n \rho_n(t), \\ N_C' = \Gamma(c, \rho_n)\rho_n + \Psi(c_1, \rho_n) \displaystyle\int_0^1 k(x) n(t, x) \mathrm{d}x, \\ c_1' = \Phi_c(c_1) c_1\,, \\ c_2' = \Phi_c(c_2) c_2\,, \end{cases} \tag{3}$$

with ρ_n defined in Eq. (2), complemented with initial conditions $n(0, x) = n^0(x)$, $c_1(0) = c_1^0$, $c_2(0) = c_2^0$, and $N_N(0) = N_C(0) = 0$, chosen to mirror experimental conditions at day 0 – see Sect. 2.2. The model accounts for:

- tumour cell proliferation, at a net growth rate given by the *growth function* $\Phi_n \geq 0$;
- baseline tumour cell death by CIK cells, independent of CAR-MET expression, at a rate given by the *baseline killing function* Γ, which is not linked to the tumour cell MET expression level x;
- additional tumour cell death due to CAR-MET.CIK cells, modulated by the MET expression levels of tumour cells, at a rate $k(x)\Psi \geq 0$, which is given by the *MET-specific killing function*, $\Psi \geq 0$, modulated by the function $0 \leq k(x) \leq 1$ encoding the impact of MET expression on MET-specific killing;
- tumour cell natural death, at a rate $\mu_n \in \mathbb{R}_{>0}$;
- CIK cell proliferation, at a net rate given by the *growth function* Φ_c, assumed to be the same for NTD.CIK and CAR-MET.CIK cells, in the light of the absence of biological evidence of a change in the doubling time of engineered CIK cells.

As detailed in the following sections, we consider different definitions for the functions Φ_n, Φ_c, Γ, and Ψ, each modelling a different hypothesis to test, identifying the ones best fitting the data via a model selection procedure described in "Model selection workflow". As regards the *MET-specific killing modulation function* $k(x)$, we assume it to be an increasing function on x, since higher MET expression of tumour cells correlates to greater killing efficacy due to an enhanced ability of CAR-MET.CIK cells to recognise their target. Further details on this function are given in Sect. 2.2.

Growth functions (Φ_n and Φ_c)

Following the idea of Benzekry et al.[38], we test three different models for the growth functions of both tumour cells, Φ_n, and CIK cells, Φ_c. Specifically, we consider:

Φ_1 - *exponential model*. Assuming that cells have an unlimited supply of space and resources, we define

$$\Phi_n(\rho_n) := \alpha_n \quad \text{and} \quad \Phi_c(c_i) := \alpha_c\,, \quad i \in \{1, 2\}\,, \tag{4}$$

where $\alpha_n \in \mathbb{R}_{>0}$ and $\alpha_c \in \mathbb{R}_{>0}$ are the rate of exponential growth of the tumour and CIK cell populations, respectively.

Φ_2 - *logistic model*. Assuming intra-population competition between cells in the same environment, each growth rate decreases linearly with the population size, i.e. we have

$$\Phi_n(\rho_n) := \alpha_n - d_n\rho_n \quad \text{and} \quad \Phi_c(c_i) := \alpha_c - d_c c_i\,, \quad i \in \{1,2\}\,, \tag{5}$$

where $\alpha_n \in \mathbb{R}_{>0}$ and $\alpha_c \in \mathbb{R}_{>0}$ represent the net proliferation rate, and $d_n \in \mathbb{R}_{>0}$ and $d_c \in \mathbb{R}_{>0}$ are the rate of cell death due to intra-population competition of the tumour and CIK cell populations, respectively.

Φ_3 - *Gompertz model*. Assuming a growth rate exponentially decaying with the population size, we define

$$\Phi_n(\rho_n) := \alpha_n - d_n \log\left(\frac{\rho_n}{\rho_n^0}\right) \quad \text{and} \quad \Phi_c(c_i) := \alpha_c - d_c \log\left(\frac{c_i}{c_i^0}\right), \quad i \in \{1,2\}\,, \tag{6}$$

where $\alpha_n \in \mathbb{R}_{>0}$ and $\alpha_c \in \mathbb{R}_{>0}$ represent the initial growth rate, and $d_n \in \mathbb{R}_{>0}$ and $d_c \in \mathbb{R}_{>0}$ are the rate of exponential decrease of the growth rate, of the tumour and CIK cell populations, respectively. Here, $\rho_n^0 = \int_0^1 n^0(x)\mathrm{d}x$ and c_i^0, $i \in \{1,2\}$, represent the initial tumour and CIK population sizes, respectively.

Note that the rate of tumour cell natural death μ_n, appearing in Eq. (3)$_2$, is incorporated in the function Φ_n via the parameter $\alpha_n = b_n - \mu_n$, with $b_n \in \mathbb{R}_{>0}$ being the cell division rate. In the *in vitro* cell proliferation assays it is clear that $b_n > \mu_n$, at least within the observed time window, motivating our choice of $\alpha_n \in \mathbb{R}_{>0}$.

Baseline CIK-mediated killing function (Γ)

We assume the baseline killing function Γ to be an increasing function of the total CIK cell number, c, given that it models the rate of tumour cell death by MET-independent CIK cell killing. We test three definitions for Γ, one of which explicitly depends on the tumour cell number ρ_n to account for the potential impact of the CIK-to-tumour ratio on the killing efficacy. Specifically, we consider scenarios in which:

Γ_1 - the killing rate is a linear function of the number of CIK cells[17], i.e.

$$\Gamma(c,\rho_n) := \gamma c\,, \tag{7}$$

where $\gamma \in \mathbb{R}_{>0}$ is the rate of tumour cell killing per CIK cell;

Γ_2 - the killing rate increases with the number of CIK cells, saturating at high CIK cell numbers, i.e.

$$\Gamma(c,\rho_n) := \gamma \frac{c}{\kappa_\gamma + c}\,, \tag{8}$$

where $\gamma \in \mathbb{R}_{>0}$ is the maximum killing rate and $\kappa_\gamma \in \mathbb{R}_{>0}$ is the half-saturation point;

Γ_3 - the killing rate increases with the CIK-to-tumour ratio, c/ρ_n, saturating as this ratio becomes large due to physical constraints or limited receptor availability[15,17,24], i.e.

$$\Gamma(c,\rho_n) := \gamma \frac{c/\rho_n}{\kappa_\gamma + c/\rho_n}\,, \tag{9}$$

where $\gamma \in \mathbb{R}_{>0}$ models the maximum killing rate and $\kappa_\gamma \in \mathbb{R}_{>0}$ is the half-saturation point.

MET-specific CIK-mediated killing function (Ψ)

We now consider the MET-specific killing function, Ψ, recalling that the total rate of tumour cell death due to MET-specific CIK-mediated killing is given by $k(x)\Psi$, with $k(x)$ modulating the MET-specific killing based on the MET expression level of tumour cells. We assume Ψ to be an increasing function of the CAR-MET.CIK cell number c_1, since only CAR-expressing CIK cells can target MET-expressing tumour cells. Following the same strategy adopted for the baseline killing function Γ, we consider the scenarios in which:

Ψ_1 - the killing rate linearly increases with the number of CAR-MET.CIK cells[17], i.e.

$$\Psi(c_1, \rho_n) := \eta c_1 \,, \tag{10}$$

where $\eta \in \mathbb{R}_{>0}$ is the maximum rate of tumour cell MET-specific killing per CAR-MET.CIK cell;

Ψ_2 - the killing rate increases with the number of CAR-MET.CIK cells increases, up to a saturation point, i.e.

$$\Psi(c_1, \rho_n) := \eta \frac{c_1}{\kappa_\eta + c_1} \,, \tag{11}$$

where $\eta \in \mathbb{R}_{>0}$ is the maximum MET-specific killing rate and $\kappa_\eta \in \mathbb{R}_{>0}$ is the half-saturation point;

Ψ_3 - the killing rate increases with the CAR-MET.CIK-tumour ratio, c_1/ρ_n, up to a saturation point[15,17,24],

$$\Psi(c_1, \rho_n) := \eta \frac{c_1/\rho_n}{\kappa_\eta + c_1/\rho_n} \,, \tag{12}$$

where $\eta \in \mathbb{R}_{>0}$ is the maximum MET-specific killing rate and $\kappa_\eta \in \mathbb{R}_{>0}$ is the half-saturation point.

MET-specific killing modulation function (k)

As previously stated, the rate of tumour cell death due to MET-specific CIK-mediated killing is modulated by the function $k(x)$, which is an increasing function of x, since higher MET expression corresponds to greater killing efficacy. For simplicity, we define $k(x)$ as a Hill function, which is widely used to model ligand-receptor binding processes and accounts for both affinity and cooperative effects[39]. In this context, it provides a flexible representation of a saturating, nonlinear response. Specifically, we define

$$k(x) = \frac{x^a}{b + x^a} \,. \tag{13}$$

with $a \in \mathbb{R}_{>0}$ and $b \in \mathbb{R}_{>0}$. In this study, we adopt $a = 0.2$ and $b = 3$, but alternative parameter values and functional forms (e.g. linear, quadratic, square root) were also considered.

Initial conditions

Tumour cell population. At day 0 of the *in vitro* cytotoxicity assays, only a percentage – denoted by $\text{MET}_{\%}$ – of the MPM cell population expresses the MET receptor. From flow cytometry analysis, we know that the MET-expression distribution of the MET-expressing subpopulation typically follows a log-normal distribution. We thus take the initial tumour cell population density function to be given by

$$n^0(x) = \rho_n^0 \left[\left(\frac{\text{MET}_{\%}}{100} \right) m^0_{\text{MET}}(x; \text{MFI}) + \left(\frac{100 - \text{MET}_{\%}}{100} \right) \delta_0(x) \right] \tag{14}$$

where $m^0_{\text{MET}}(x; \text{MFI})$ models the rescaled MET-expression distribution of the MET-expressing subpopulation at day 0, while $\delta_0(x)$ denotes the Dirac delta distribution centered at $x = 0$, which corresponds to the other $100 - \text{MET}_{\%}$ percentage of tumour cells not expressing the MET receptor. We take $m^0_{\text{MET}}(x; \text{MFI})$ to be a log-normal distribution, with mode given by the rescaled experimental MFI (i.e. $x_{\text{MFI}} := \text{MFI}/y_H$).

CIK cell population. Similarly, we know from experiments that only a percentage – denoted by $\text{CAR}_{\%}$ – of the CIK population presents the CAR-MET after genetic engineering. Therefore, given the initial number of CIK cells, c^0, we define the initial CAR-MET.CIK and NTD.CIK cell numbers respectively as

$$c_1^0 = \frac{\text{CAR}_{\%}}{100} c^0 \qquad \text{and} \qquad c_2^0 = c^0 - c_1^0. \tag{15}$$

Reproducing *in vitro* assays. When reproducing *in silico* the experimental cell growth and cytotoxicity assays, we take the MPM cell line-specific $MET_{\%}$ and MFI, the CIK preparation-specific $CAR_{\%}$, and initial tumour cell number, ρ_n^0, and CIK cell number, c^0, specific to the considered experiment. In cytotoxicity assays, the quantity c^0/ρ_n^0 corresponds to the experimental E:T ratio.

Numerical TSK

Similarly to the TSK formula introduced in Eq. (1) to quantify the percentage of tumour-specific lysis observed during experiments, we introduce its *in silico* counterpart, that is, the numerical TSK, $f_{\mathrm{TSK}}(t)$, defined as

$$f_{\mathrm{TSK}} = \frac{f_{\mathrm{E}} - f_{\mathrm{S}}}{100 - f_{\mathrm{S}}} \times 100, \text{ where } f_{\mathrm{E}} = \frac{N_C^E + N_N^E}{N_C^E + N_N^E + \rho_n^E} \times 100 \text{ and } f_{\mathrm{S}} = \frac{N_N^S}{N_N^S + \rho_n^S} \times 100. \tag{16}$$

Here, N_C^E, N_N^E, and ρ_n^E denote N_C, N_N, and ρ_n obtained by simulating the model in the presence of CIK cells, such that f_E is the numerical counterpart of the *experimental mortality* in Eq. (1). Moreover, N_N^S and ρ_n^S denote N_N and ρ_n obtained by re-running the simulation in the absence of CIK cells, i.e. setting $c^0 = 0$, such that f_S is the numerical counterpart of the *spontaneous mortality* in Eq. (1).

Model selection and calibration

Following the approach of Benzekry et al.[38], we compare the proposed definitions for Φ_n, Φ_c, Γ, and Ψ, introduced in the previous section, to select those that provide the best fit for the majority of MPM cell lines and CIK cell preparations. Once the most accurate version of the model is established, we carry out model calibration[32,38,40] to obtain a distribution of values for each parameter, capturing their variability among different MPM cell lines and CIK preparations.

Model selection methodology

To select the most appropriate definition for each of the functions appearing in the model, we compare the AIC of each candidate, which is calculated from the corresponding maximum likelihood estimate (MLE). We do this separately for each cell line – or, in the case of TSK data, for each MPM-CIK combination – and ultimately select the model best fitting the majority of cell lines.

Maximum likelihood estimation. To estimate the parameter set yielding the MLE, we adopt the Weighted Least Square (WLS) optimisation method[38,41]. In particular, we view the experimental data as realisations of the random variables $y_{i,j}$ (at time t_i, under experimental condition E_j) generated by the deterministic model with output $f_k^i(\theta, E_j)$ (at time t_i, with candidate model k, parameter set θ, and under experimental condition E_j) and perturbed by a random effect. We assume the latter to be Gaussian, with standard deviation selected *ad hoc* for each experiment (see Supp. Mat. S.1.1). In order to compute $f_k^i(\theta, E_j)$, we numerically simulate the corresponding system by adopting the MATLAB solver *ode45*, which encodes an explicit Runge-Kutta scheme. Moreover, to find the optimal parameter set (OPS), $\hat{\theta}$, we employ the pre-implemented MATLAB function *lsqcurvefit*[42]. For the parameter set domain, we consider parameter ranges reported in the literature (see Supp. Mat. Table S.1).

Model comparison and selection. As similarly done in[43], for each experimental condition E_j – i.e. MPM cell line, CIK preparation or MPM-CIK combination – and candidate model k, we use the obtained MLEs to calculate the AIC and corresponding Akaike Weight (AW), see Supp Mat. S.2.2 for details. The AIC is a well-known method for evaluating how well a model fits the data and for comparing candidate models of varying complexity, penalising those that rely on a large number of parameters, with the optimal candidate identified as the one exhibiting the lowest AIC[34,43]. The AWs, which sum up to one, can be interpreted as the probability that a given model is the best among the candidates, conditional on the observed data. Therefore, they quantify the degree to which the model with the lowest AIC outperforms the alternative options (i.e. the larger the AW of a candidate model is

compared to the AWs of the other models, the stronger the candidate). The function that provides the best fit for the majority of cell lines (or CIK preparations, or MPM-CIK combinations) is selected as the final model.

Model selection workflow

Full model selection is conducted by considering specific sub-models, corresponding to well-defined experimental scenarios, in which the model defined via Eqs. (3) simplifies and allows for a direct comparison with the available experimental data. In particular, we select the final model by proceeding as described below.

(I) **Growth functions (Φ) selection.** We first select the best model for Φ_n and Φ_c (among Φ_1, Φ_2, and Φ_3 introduced in Sect. 2.2) by simulating the proliferation assays (cf. "Cell growth assay") in which the tumour and CIK populations evolve independently. In these simulations, both the baseline and MET-specific CIK-mediated killing terms are null (i.e. $\Gamma \equiv 0$ and $\Psi \equiv 0$).

(II) **Natural death rate (μ_n) estimation.** Given the selected definitions of Φ_n and Φ_c, we fix for each cell line the corresponding OPS. Focusing on Eqs. (3) under the scenario $c^0 = 0$ (yielding $c_1(t) = c_2(t) = 0$ for all $t \geq 0$), and the selected definition of Φ_n, we obtain an analytical formulation for the natural death rate μ_n (see Supp. Mat. S.1.4), which depends on N_N. Then, we evaluate the number of tumour cells that died due to natural causes, i.e. the experimental counterpart of N_N, after 2 days from the cancer cell growth data ("Cell growth assay") and the *spontaneous mortality* data ("In vitro cytotoxicity assays"), using the formula of the numerical counterpart of this quantity, f_S, defined in Eq. (16). This gives an estimate for μ_n for each MPM cell line, which we fix alongside the selected growth functions and OPSs.

(III) **Baseline CIK-mediated killing function (Γ) selection.** We then select the best definition of Γ (among Γ_1, Γ_2, and Γ_3 introduced in Sect. 2.2) by comparing the NTD.CIK *experimental mortality- spontaneous mortality* data of Sect. 2.1 with the corresponding model output, i.e. $f_E - f_S$ in Eq. (16), evaluated at $t = 2$ days, under the scenario $c_1^0 = 0$ (i.e. $c_1(t) = 0$ and $c(t) = c_2(t)$ for all $t \geq 0$).

(IV) **MET-specific CIK-mediated killing function (Ψ) selection.** Given the selected Γ function, we fix for each MPM-CIK combination the corresponding OPS. We select the best choice for Ψ (among Ψ_1, Ψ_2 , and Ψ_3 introduced in Sect. 2.2) by simulating the full model defined via Eqs. (3), and comparing the model output $f_E - f_S$ in Eq. (16) with its experimental counterpart (cf. data of Sect. 2.1) in the presence of CAR-MET.CIK cells. We remark that at this stage the definition of the function $k(x)$ fixed in Sect. 2.2 does not significantly affect the goodness of fit, since the model is calibrated separately for each cell line, but rather the range of values in the OPS of the parameters appearing in the function Ψ.

Bayesian inference of the selected model

As commonly conducted in biological system studies[32,40,44,45], we perform Bayesian inference on the selected model, to carry out practical identifiability analysis (i.e. to assess the ability of the method to truly identify parameter values from the available data)[32] and to quantify uncertainty in parameter estimates and model predictions. This is achieved by adopting a Markov Chain Monte-Carlo (MCMC) approach, employing the Python package PINTS[46]. For this procedure, we consider the cell growth data described in Sect. 2.1 and the TSK data introduced in Sect. 2.1, comparing them with the corresponding model output, that is, ρ_n, c_1, c_2, and f_{TSK} defined in Eq. (16). In the absence of prior information on the parameter values, we consider a weakly-informative uniform prior distribution for each parameter. In particular, we set uniform prior distributions, with lower and upper bounds – reported in Table 4 – chosen based on the parameter values found during the model selection phase. More details on the calibration setup are provided in Supp. Mat. S.1.3. We also remark that a reparametrisation ($\hat{\gamma} = \gamma/\kappa_\gamma$ and $\hat{\eta} = \eta/\kappa_\eta$) has been applied prior to the final calibration – further details on this can be found in Sect. 3.2. Posterior distributions of the parameter values are then used to obtain the 95% and 68% Confidence Intervals (CIs) of model outputs, as well as the the mean estimate (ME) – i.e. the mean of model outputs – as similarly done in[40].

Results

Model selection reveals underlying biological mechanisms

MPM and CIK cell populations grow exponentially

Step (I) of the model selection procedure – which leads to the selection of Φ_1 – reveals that cell population growth follows an exponential trend, both in MPM and CIK cells, at least over the observed experimental time window. While the unlimited population growth assumption is not reasonable in real-life conditions, it is commonly adopted for short experimental time horizons, as the one considered in this study.

The AIC values and corresponding AWs are reported in Table 1, while comparisons between model predictions for the different model candidates (Φ_1, Φ_2, and Φ_3) and experimental data of MPM and CIK cell growth assays are shown in Fig. 2a,b, respectively, for a representative MPM cell line (NCI-H28) and a representative NTD.CIK preparation (NTD.CIK A). We see from Table 1 that for the majority of MPM cell lines and CIK preparations, the exponential growth model (i.e. Φ_1) significantly outperforms the other two candidates according to the selection criteria. A few exceptions can be observed: the MSTO-211H cell line favours the logistic model, while the NTD.CIK B, NTD.CIK D and CAR-MET.CIK D favour the Gompertz model. However, in these cases, a visual comparison of the model outputs indicates that the difference between the fitted curves are negligible (cf. Supp. Mat. Figures S.2 and S.3). Therefore, we select the exponential growth model Φ_1 for both the tumour and CIK growth functions.

The baseline CIK-mediated killing rate depends on the CIK-to-tumour cells ratio

Step (III) of the model selection procedure – which leads to the selection of Γ_3 – reveals that the baseline CIK-mediated killing rate depends on the ratio of CIK cells to tumour cells and saturates with this ratio. This is reasonable, since tumour cells possess a limited number of NKG2D ligands mediating the intrinsic CIK killing activity

Table 1 Cell growth model selection.

Model selection results for the growth functions Φ_n and Φ_c

	AIC (AW)		
MPM (Φ_n)	**Exponential** Φ_1	**Logistic** Φ_2	**Gompertz** Φ_3
NCI-H28	18.91(0.58)	20.91 (0.21)	20.91 (0.21)
Nominated SPC-212	18.35(0.58)	20.35 (0.21)	20.35 (0.21)
MSTO-211H	13.37 (0.25)	12.27(0.44)	12.93 (0.31)
NCI-H2052	18.70(0.58)	20.70 (0.21)	20.70 (0.21)
MERO-25	16.70(0.58)	18.70 (0.21)	18.70 (0.21)
CIK (Φ_c)	**Exponential** Φ_1	**Logistic** Φ_2	**Gompertz** Φ_3
NTD.CIK A	16.73(0.58)	18.73 (0.21)	18.73 (0.21)
NTD.CIK B	9.62(0.73)	21.21 (0.00)	11.62 (0.27)
NTD.CIK C	31.99 (0.07)	28.18 (0.46)	28.10(0.47)
NTD.CIK D	15.38 (0.00)	24.76 (0.00)	5.08(0.99)
CAR-MET.CIK A	16.16(0.60)	18.56 (0.18)	18.16 (0.22)
CAR-MET.CIK B	14.86(0.70)	20.43 (0.04)	16.86 (0.26)
CAR-MET.CIK C	16.86(0.59)	19.11 (0.19)	18.86 (0.22)
CAR-MET.CIK D	11.68 (0.15)	26.06 (0.00)	8.17(0.85)

AIC values, and related AWs, corresponding to different growth function models (Φ_1, Φ_2, and Φ_3) for each MPM cell line (selecting Φ_n) and CIK preparation (selecting Φ_c), with the lowest AIC (and corresponding AW) highlighted in bold. These results have been obtained through the model selection procedure described in Sect. 2.3, with step (I) of the procedure described in Sect. 2.3, i.e. the MLEs used to compute the AICs and AWs are obtained by calibrating the model defined via Eqs. (3), setting $\Gamma = 0$ and $\Psi = 0$, with data from cell growth assays described in Sect. 2.1.

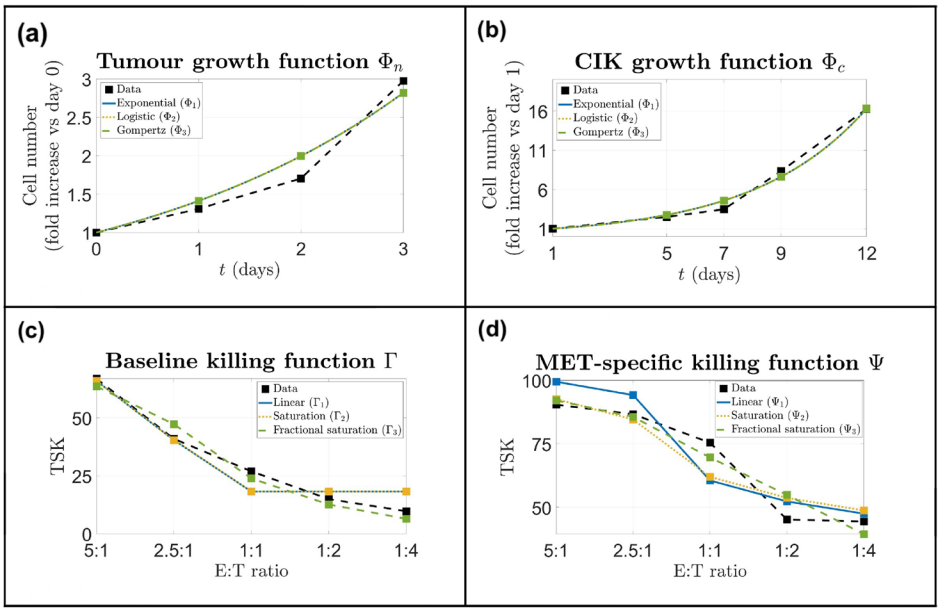

Figure 2 Model selection results. Graphic comparison between data of representative MPM cell lines and CIK preparations (black squares) with model outputs under different definitions (coloured curves) of the functions Φ_n (**a**), Φ_c (**b**), Γ (**c**), and Ψ (**d**), introduced in Sect. 2.2-2.2, obtained with the methods of Sect. 2.3-2.3. Panels display: (**a**) MPM (NCI-H28 cell line) cell numbers and ρ_n, normalised at day 0, over time; (**b**) CIK (NTD.CIK A) cell numbers and c_2, normalised at day 1, over time; (**c**) TSK (NCI-H28 vs NTD.CIK B) and f_{TSK} at day 2 in a control scenario (no engineering, i.e. $c_1^0 = 0$) under different initial E:T (i.e. c^0/ρ_n^0) ratios; (**d**) TSK (NCI-H28 vs CAR-MET.CIK B) and f_{TSK} at day 2 post-engineering under different initial E:T ratios. See Supp. Mat. Figures S.2-S.5 for model selection plots of each experiment.

and, therefore, once the number of CIK cells available per cancer cell exceeds this limit, further increases do not meaningfully enhance the rate at which tumour cells are killed by CIK cells.

The AIC values, and corresponding AWs, of the three model candidates for the baseline killing function Γ are reported in Table 2, where we see that the function Γ_3 significantly outperforms the other candidates for most combinations of MPM cell lines and NTD.CIK preparations, with Γ_1 being a strong second candidate. Yet, as it can be seen in Fig. 2c, for a representative combination of MPM cell line and NTD.CIK preparation (NCI-H28 vs NTD.CIK B), the fractional saturation assumption encoded in the definition of Γ_3 is the only one that can capture the experimental TSK trends of NTD.CIK cytotoxicity assays at lower initial E:T ratios. This is due to the fact that, when $\Gamma \equiv \Gamma_1$ or $\Gamma \equiv \Gamma_2$, the numerical TSK f_{TSK} does not depend on the initial number of tumour cells. On the basis of these results, we select the fractional saturation model Γ_3 for the baseline CIK-mediated killing function.

The MET-specific CIK-mediated killing rate depends on the CIK-to-tumour cells ratio

Similarly to as concluded for the baseline killing, step (IV) of the model selection procedure, which leads to the selection of Ψ_3, reveals that the killing elicited upon the engagement of MET by the CAR expressed on the CIK surface depends on the ratio of CAR-MET.CIK cells to tumour cells and, reasonably, saturates with this ratio. This is again consistent with the physical constraints of ligand-receptor dynamics previously discussed in Sect. 3.1.

The AIC values, with corresponding AWs, of the three versions of the function Ψ are reported in Table 3, where it is clear that Ψ_3 outperforms other candidate models for all MPM-CIK combinations. A graphical comparison between model predictions (for Ψ_1, Ψ_2, and Ψ_3) of f_{TSK} and experimental TSK obtained in CAR-MET.CIK cytotoxicity assays are displayed in Fig. 2d for a representative combination of an MPM cell line and a CAR-MET.CIK preparation (NCI-H28 vs CAR-MET.CIK B). In the light of these results, we select the fractional saturation

Table 2 Baseline CIK-mediated killing model selection.

AIC values, and related AWs, corresponding to different baseline killing function definitions (Γ_1, Γ_2, and Γ_3) for each combination of MPM cell line and NTD.CIK preparation, with the lowest AIC (and corresponding AW) highlighted in bold. These results have been obtained through the model selection procedure described in Sect. 2.3, with step (III) of the procedure described in Sect. 2.3, i.e. the MLEs used to compute the AICs and AWs are obtained by calibrating the model defined via Eqs. (3), setting $c_1^0 = 0$, with data from cytotoxicity assays with NTD.CIK cells described in Sect. 2.1.

Model selection results for the baseline killing function Γ				
	AIC (AW)			
CIK	NTD.CIK A	NTD.CIK B	NTD.CIK C	NTD.CIK D
MPM	**Linear Γ_1**			
NCI-H28	24.54 (0.00)	21.32 (0.26)	13.04(0.72)	–
SPC-212	14.89(0.55)	23.68 (0.06)	–	25.30 (0.00)
MSTO-211H	19.93(0.43)	23.38(0.62)	–	22.01 (0.38)
NCI-H2052	–	8.62 (0.20)	14.94 (0.02)	5.95 (0.02)
MERO-25	20.06 (0.01)	–	24.15 (0.00)	23.70 (0.00)
MPM	**Saturation Γ_2**			
NCI-H28	26.54 (0.00)	23.32 (0.10)	15.04 (0.26)	–
SPC-212	15.55 (0.39)	25.68 (0.02)	–	27.30 (0.00)
MSTO-211H	21.93 (0.16)	25.37 (0.23)	–	24.01 (0.14)
NCI-H2052	–	10.62 (0.08)	16.94 (0.02)	3.15 (0.08)
MERO-25	22.06 (0.01)	–	26.15 (0.00)	25.70 (0.00)
MPM	**Fractional saturation Γ_3**			
NCI-H28	8.44(0.99)	19.57(0.64)	20.08 (0.02)	–
SPC-212	19.22 (0.06)	18.11(0.92)	–	8.86(0.99)
MSTO-211H	20.06 (0.41)	26.29 (0.15)	–	21.49(0.48)
NCI-H2052	–	6.13(0.72)	7.73(0.96)	-1.67(0.90)
MERO-25	11.76(0.98)	–	14.05(0.99)	7.67(0.99)

Table 3 MET-specific CIK-mediated killing model selection.

AIC values, and related AWs, corresponding to different MET-specific killing function definitions (Ψ_1, Ψ_2, and Ψ_3) for each combination of MPM cell line and CAR-MET.CIK preparation, with the lowest AIC (and corresponding AW) highlighted in bold. These results have been obtained through the model selection procedure described in Sect. 2.3, with step (IV) of the procedure described in Sect. 2.3, i.e. the MLEs used to compute the AICs and AWs are obtained by calibrating the model defined via Eqs. (3) with data from post-engineering cytotoxicity assays described in Sect. 2.1.

Model selection results for the MET-specific killing function Ψ				
	AIC (AW)			
CIK	CAR-MET.CIK A	CAR-MET.CIK B	CAR-MET.CIK C	CAR-MET.CIK D
MPM	**Linear Ψ_1**			
NCI-H28	25.94(0.57)	25.49 (0.16)	23.07 (0.01)	–
SPC-212	26.09 (0.04)	31.05 (0.03)	–	31.16 (0.18)
MSTO-211H	27.10 (0.03)	19.68 (0.10)	–	28.57 (0.00)
NCI-H2052	–	21.58 (0.00)	31.14 (0.01)	18.37 (0.18)
MERO-25	17.27(0.55)	–	20.46 (0.02)	15.20 (0.26)
MPM	**Saturation Ψ_2**			
NCI-H28	27.93 (0.21)	25.48 (0.16)	23.01 (0.01)	–
SPC-212	23.19 (0.18)	33.05 (0.01)	–	29.71 (0.38)
MSTO-211H	24.04 (0.14)	20.51 (0.06)	–	29.07 (0.00)
NCI-H2052	–	23.58 (0.00)	33.14 (0.00)	20.37 (0.07)
MERO-25	19.25 (0.20)	–	22.46 (0.00)	14.74 (0.32)
MPM	**Fractional saturation Ψ_3**			
NCI-H28	27.87 (0.22)	22.56(0.68)	12.96(0.98)	–
SPC-212	20.22(0.78)	23.81(0.96)	–	29.42(0.44)
MSTO-211H	20.40(0.83)	15.38(0.84)	–	17.29(0.99)
NCI-H2052	–	7.99(0.99)	22.15(0.98)	15.54(0.75)
MERO-25	18.91 (0.25)	–	12.28(0.98)	14.20(0.42)

model Ψ_3 for the MET-specific killing function, establishing the final version of the mathematical model. This consists of Eqs. (3), complemented with the definitions given by Eqs. (2), (4), (9), (12), and (13), subject to the initial conditions defined via Eqs. (14) and (15).

Bayesian inference of the selected model reveals treatment efficacy

Practical identifiability is achieved for most parameters of the selected model

Bayesian inference reveals that practical identifiability is achieved for most parameters of the selected model, as demonstrated by the fact that the estimated marginal posterior distributions, shown in Fig. 3b, exhibit a unique and well-defined maximum for most parameters – see also the corresponding summary statistics in Table 4. Note that the posterior analysis required a re-parametrisation of the model, introducing $\hat{\gamma} = \gamma/\kappa_\gamma$ and $\hat{\eta} = \eta/\kappa_\eta$, due to strong posterior positive correlations between the two parameters within each fractional saturation term, i.e. Γ_3 and Ψ_3. While some degree of correlation between $\hat{\gamma}$ and κ_γ, or $\hat{\eta}$ and κ_η, is still observed in joint posterior distributions, these present clearly identifiable maxima. In particular, the marginal posteriors of $\hat{\gamma}$ and $\hat{\eta}$, as well as those of α_n and α_c, display approximately bell-shaped profiles, whereas those of κ_γ, and κ_η are right-skewed. In contrast, the posterior distribution of μ_n is characterised by a broad support, indicating substantial uncertainty in the estimation of the MPM natural death rate.

The calibrated model captures data variability across cell lines and helps identify outliers

By sampling from the posterior distributions, the 95% CI of the calibrated model output reflects variability across MPM cell lines and CIK preparations, as shown in Fig. 3a. In particular, model uncertainty in predicting cell counts grows over time (cf. first two panels), while uncertainty in predicting the NTD.CIK TSK decreases along with the E:T ratio (cf. third panel). In the last column of Fig. 3a, we can observe great variability in the TSK across experiments with different CAR-MET.CIK preparations, characterised by different $CAR_{\%}$ levels, for each MPM cell line. This variability is loosely captured by the model, the width of the 95% CI of which remains approximately constant across E:T ratios, and it is larger in MPM cell lines with higher MET expression level – i.e. greater MFI and $MET_{\%}$. This suggests that the numerical TSK becomes more sensitive to variations in CIK $CAR_{\%}$ as the MET expression level of MPM cells increases.

The 95% CI of the calibrated model outputs also highlights which MPM cell lines and CIK preparations display outlier behaviour compared to the general trend – cf. orange markers in the first three panels of Fig. 3a. The MSTO-211H and the NTD.CIK D exhibit higher growth rates than the other MPM cell lines and CIK cell preparations, while the NCI-H2052 cell line exhibits a TSK that is notably lower than average in NTD.CIK cytotoxicity assays. For highly MET expressing MPM cell lines (NCI-H28 and SPC-212), TSK data in CAR-MET.CIK cytotoxicity assays are entirely contained within the 95% CI of the numerical TSK, with medians closely aligned with the ME. The agreement is weaker for MPM cell lines with lower MET expression, with the NCI-H2052 cell line displaying a TSK consistently lower than average, likely due to the fact that its baseline killing is already poorly captured.

CAR-MET.CIK engineering and higher $CAR_{\%}$ improve treatment efficacy

As expected, the results in Fig. 3a indicate that higher initial E:T ratios result in higher (experimental and numerical) TSK in both NTD.CIK and CAR-MET.CIK cytotoxicity assays. Remarkably, we see that, both in experimental data and in calibrated model outputs, TSK values in NTD.CIK cytotoxicity assays are consistently lower than those obtained with CAR-MET-CIK cells, across all E:T ratios and regardless of MET expression levels. This is consistent with the biological notion motivating CAR-MET.CIK engineering, confirming that CAR expression targeting the MET receptor on MPM cells enhances the tumour-killing efficacy of CIK cells. Moreover, as shown by Fig. 4a, the calibrated model predicts that a higher $CAR_{\%}$ upon CIK cell engineering results in higher TSK levels. This trend is also observed in experimental data, as shown by Fig. 3c for the NCI-H28 cell line and different CIK preparations of increasing $CAR_{\%}$, illustrating a pattern shared by all cell lines (see Supp. Mat. Figure S.7). Ultimately, the $CAR_{\%}$ obtained upon engineering may determine whether a CIK cell preparation will yield a

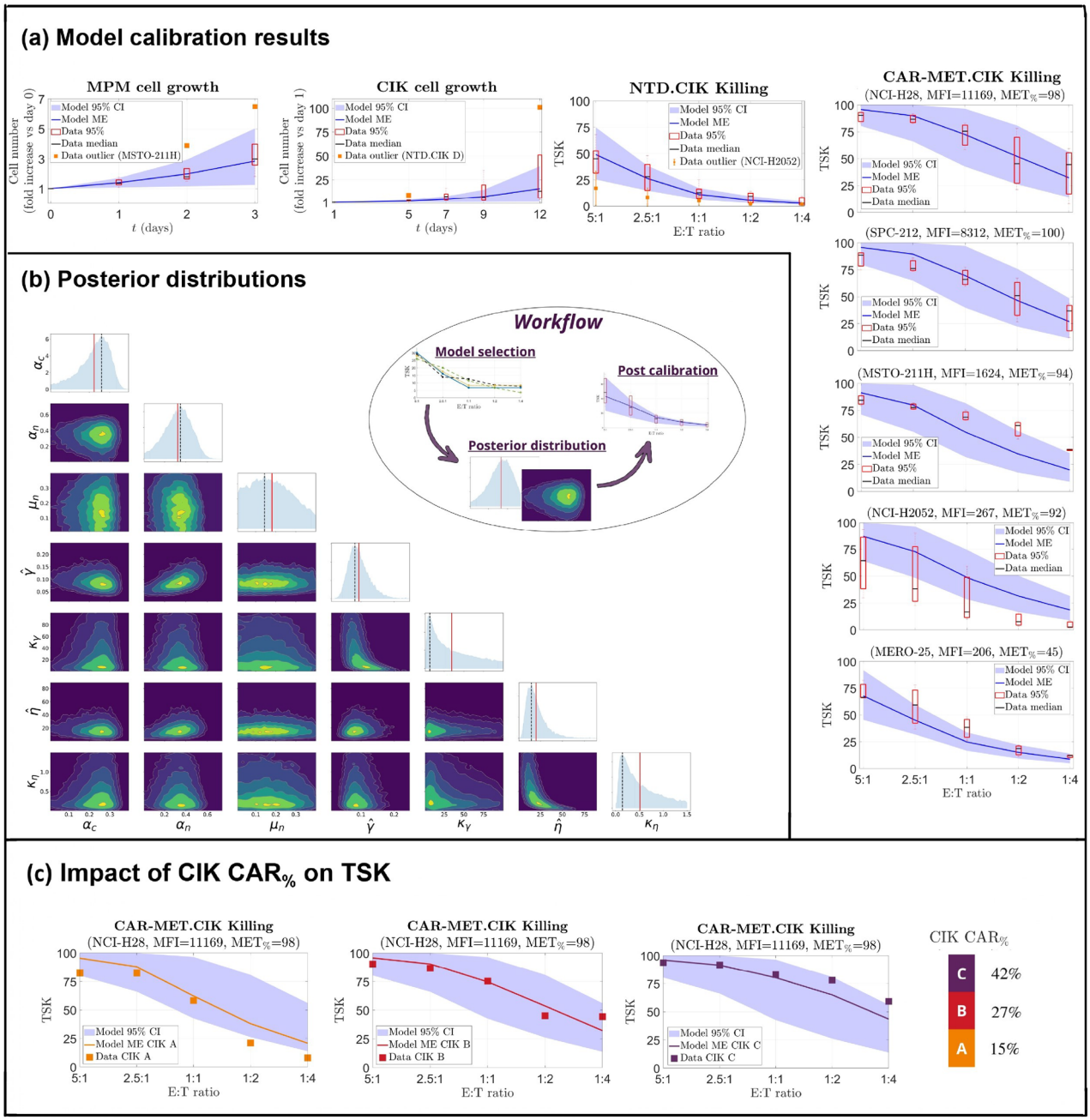

Figure 3 Model calibration results. Calibrated model predictions and parameter distributions obtained through the procedure described in Sect. 2.3 – cf. subplot (**b**) for the calibration procedure. (**a**) Post calibration fit comparing data across all cell lines (left and central panels, red boxplots with black median, outlier data marked in orange) and selected model outputs after Bayesian inference (solid blue lines highlight the ME, light blue shaded areas highlight the 95% CI). Panels left-to-right display the same quantities as in the panels (a–c) of Figure 2, reproducing, respectively, MPM and CIK cell growth assays and NTD.CIK cytotoxicity assays. Panels in the right column display TSK and f_{TSK} at day 2 of CAR-MET.CIK cytotoxicity assays, as in Fig. 2d, for each MPM cell line separately (red boxplots highlight data variability across 3 replicates, with different $\mathrm{CAR}_{\%}$, of each cytotoxicity assay), with tumour cell MFI from highest to lowest (top-to-bottom). (**b**) Posterior distributions of the parameters obtained through the calibration procedure. The diagonal panels display the marginal posterior distributions (mean value and mode are highlighted by the solid red and dashed black lines, respectively) – see Table 4 for summary statistics. **(c) Impact of $\mathrm{CAR}_{\%}$ on TSK** of CAR-MET.CIK cytotoxicity assays of a representative cell line (NCI-H28) and CIK A ($\mathrm{CAR}_{\%}$ = 15, in orange, left panel), B ($\mathrm{CAR}_{\%}$ = 27, in red, central panel) and C ($\mathrm{CAR}_{\%}$ = 42, in purple, right panel). Experimental TSK (coloured squares) and the ME of f_{TSK} (solid coloured lines) at day 2 of cytotoxicity assays are displayed for each CIK preparation, along with the corresponding 95% CI (light blue shaded area).

Table 4 Summary statistics of parameter posterior distributions.

Parameters		Prior		Posterior					OPS
θ	unit	$\mathcal{U}$-lb	$\mathcal{U}$-ub	mean	std	mode	$Q_{2.5\%}$	$Q_{97.5\%}$	$\hat{\theta}$
α_c	1/day	0.01	1	0.227	0.073	0.261	0.070	0.343	0.27
α_n	1/day	0.01	1	0.325	0.124	0.344	0.076	0.550	0.38
μ_n	1/day	0.01	0.4	0.179	0.100	0.144	0.010	0.358	0.13
$\hat{\gamma}$	1/day	0.01	0.25	0.093	0.031	0.082	0.041	0.158	0.13
κ_γ	no unit	0.1	100	35.929	27.813	7.254	1.242	90.376	4.64
$\hat{\eta}$	1/day	0.01	90	21.002	12.226	13.151	4.110	47.001	23.02
κ_η	no unit	0.001	1.5	0.508	0.385	0.121	0.025	1.282	0.18

Summary statistics for the marginal posterior distributions, obtained through the procedure described in Sect. 2.3, of the parameters in the model defined via Eqs. (3) with the selected functions Φ_1 (for both Φ_n and Φ_c), Γ_3, and Ψ_3, i.e. definitions given by Eqs. (4), (9), and (12). For each parameter, we provide the unit, the lower and upper bounds of the uniform prior distribution, the mean, standard deviation and mode, as well as the quantiles $Q_{2.5\%}$ and $Q_{97.5\%}$, of the posterior distribution – see also Fig. 3b. We also provide the value of the parameter in the OPS, $\hat{\theta}$, obtained via the WLS method, considering all data simultaneously.

clinically meaningful increase in tumour killing. For example, Fig. 3c shows that, at an initial E:T ratio of 1:2, TSK = 21.1 for CAR-MET.CIK A ($CAR_{\%} = 15$) while TSK = 78.1 for CAR-MET.CIK C ($CAR_{\%} = 42$).

High MET-expressing cell lines exhibit the greatest enhancements in treatment efficacy

While the general TSK trends described in Sect. 3.2 are common to all MPM cell lines, differences in initial MET expression give rise to distinct CAR-MET.CIK TSK profiles, as can be observed in the right column of Fig. 3a. Overall, the increase in TSK when switching from NTD.CIK to CAR-MET.CIK is far greater in cell lines with high (cf. MSTO-211H, mid panel) and very high (cf. NCI-H28 and SPC-212, top panels) MET expression, compared to those with intermediate MET expression levels (cf. NCI-H2052 and MERO-25, bottom panels). At low E:T ratios, MPM cell lines with lower MFI do not exhibit any significant increase in TSK when CIK preparations with higher $CAR_{\%}$ are employed. For these, meaningful results are only obtained at (clinically-impractical) high E:T ratios. Conversely, MPM cell lines with very high MET expression are particularly sensitive to $CAR_{\%}$ changes even al low E:T ratios – see also Fig. 3c. Moreover, for these cell lines, TSK levels are consistently high at higher E:T ratios, independently of $CAR_{\%}$. These trends are also captured by the calibrated model.

Taken together, these results suggest that the MET expression level, summarised by the MFI and $MET_{\%}$ of a given MPM cell line, may be a strong indicator of whether we can expect clinically meaningful results with CAR-MET.CIK cell immunotherapy.

Model predictions on treatment efficacy are validated with primary cell lines

In Sect. 3.2 we discussed how the calibrated model can capture the impact of $CAR_{\%}$ upon engineering, MET expression of MPM cells, and the initial E:T ratio on the efficacy of CAR-MET.CIK treatment – quantified by the TSK defined via Eq. (1) – observed during experiments. We thus propose the mathematical model as a quantitative tool to predict treatment efficacy prior to administration, and validate model predictions with three MPM primary cell lines – covering intermediate and high MET expression levels – and three new CIK preparations.

The calibrated model may help achieve pre-set treatment efficacy targets

For a given MPM cell population, characterised by its MFI and $MET_{\%}$, the calibrated model can be used to generate a heatmap of predicted TSK, i.e. the numerical f_{TSK}, for different $CAR_{\%}$ and E:T ratios, as shown in Fig. 4a. These heatmaps summarise the previously discussed biological findings on the TSK trends. Once chosen a specific therapeutic target, e.g. TSK = 85 after 3 days of treatment, the heatmaps help identify the minimum E:T ratio required to achieve the desired TSK for a given MPM cell line and CIK $CAR_{\%}$. For instance, after engineering

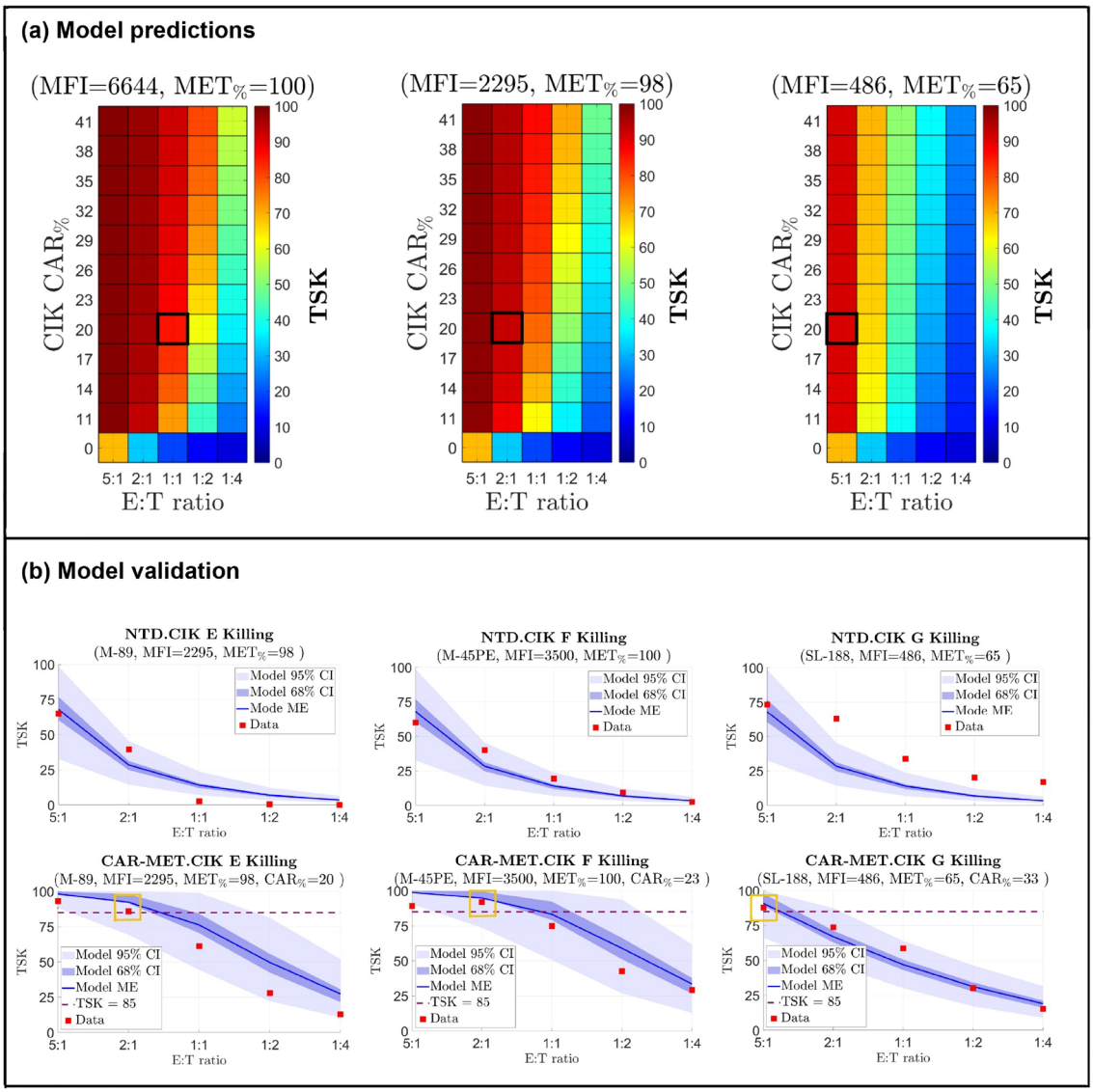

Figure 4 Calibrated model predictions and validation. Model prediction obtained through the procedure described in Sect. 2.3 and post-calibration parameter distributions displayed in Fig. 3b with summary statistics in Table 4. (**a**) Model prediction of TSK heat maps, for different initial E:T ratios (*x*-axis) and CIK $CAR_{\%}$ (*y*-axis), corresponding to MPM cell lines with very high (MFI = 6644 and $MET_{\%}$ = 100), high (MFI = 2295 and $MET_{\%}$ = 98), and intermediate (MFI = 486 and $MET_{\%}$ = 65) MET expression levels, respectively (left-to-right). Specific values of MFI and $MET_{\%}$ have been chosen to exhibit a range of MET expression levels (intermediate, high, very high), and match a few of the MPM primary cell lines used for validation. Black squares mark TSK ≈ 85, chosen to showcase how model predictions may help attain a selected therapeutic target. (**b**) Validation of model predictions with the MPM primary cell lines and new CIK preparations. NTD.CIK and CAR-MET.CIK (resp. top and bottom rows) cytotoxicity assays are reproduced for the following combinations of MPM cell line and CIK preparation (resp. left-to-right columns): M-89 (MFI = 2295 and $MET_{\%}$ = 98) and CIK E ($CAR_{\%}$ = 20); M-45PE (MFI = 3500 and $MET_{\%}$ = 100) and CIK F ($CAR_{\%}$ = 23); SL-188 (MFI = 486 and $MET_{\%}$ = 65%) and CIK G ($CAR_{\%}$ = 33). Panels display the experimental TSK (red squares) and numerical f_{TSK} at day 3 of the cytotoxicity assays, with the solid blue line highlighting the ME, and shaded areas highlighting the 95% and 68% CI (resp. light blue and blue). Dashed purple lines highlight TSK = 85, chosen to showcase how model predictions may help attain a selected therapeutic target, and yellow squares highlight the data validating such prediction.

CAR-MET.CIK E, which was transduced with $CAR_{\%} = 20$, we expect a TSK of 85 after 3 days to be attainable in the MPM primary cells lines with: very high MET expression, by choosing an E:T ratio of at least 1:1; high MET expression, by choosing an E:T ratio of at least 2:1; intermediate MET expression under an E:T ratio of at least 5:1 – cf. black squares in, respectively, left-to-right heatmaps of Fig. 4a.

This prediction was validated *in vitro* for the MPM primary cell line M-89, with MFI = 2295 and $MET_{\%} = 98$ exactly as in the central heatmap, for which an experimental TSK of approximately 85 is attained with an E:T ratio of at least 2:1, as predicted by the model – cf. yellow square in the CAR-MET.CIK E Killing panel of Fig. 4b. Similar model predictions, for the same treatment efficacy target, were also validated in other MPM primary cell lines: the M-45PE cell line (also exhibiting high levels of MET expression) against the CAR-MET.CIK F preparation ($CAR_{\%} = 23$), and the SL-188 cell line (with intermediate levels of MET expression – MFI and $MET_{\%}$ exactly as in the right heatmap of Fig. 4a) against the CAR-MET.CIK G preparation ($CAR_{\%} = 33$). The respective predictions are validated by the experimental data, as highlighted by the yellow squares of the corresponding CAR-MET.CIK Killing panels.

Qualitative TSK trends are validated in MPM primary cell lines

To further test the robustness of the calibrated model predictions, we conducted both NTD.CIK and CAR-MET.CIK cytotoxicity assays on the MPM primary cell lines for different initial E:T ratios, on top of the ones required for validation of the model prediction example of Sect. 3.3. The experimental TSK data, which are plot against the calibrated model outputs in Fig. 4b, are fully contained in the 95% CI of the numerical TSK predicted in CAR-MET.CIK cytotoxicity assays, even when the fit is not as close in the corresponding NTD.CIK cytotoxicity assays (cf. panels in the left and right columns), a promising result for a potential predictive use of the model. We acknowledge that model predictions may not be as accurate for a range of lower TSK targets, as indicated by some data points falling outside the 68% CI of model outputs, likely due to the fact that the model was calibrated with data from commercial cell lines and over a time window that was one day shorter than the validation data. Nevertheless, we stress that the experimental TSK profiles of the MPM primary cell lines exhibit the same qualitative behaviour observed in the commercial ones and in the calibrated model outputs.

Discussion

Model performance

In this paper, we adopted an experimentally-informed mathematical modelling approach to investigate the efficacy of CAR-MET.CIK cells against MPM cells. By integrating data from cytotoxicity experiments in the model, performing model selection and uncertainty quantification via Bayesian inference, the framework provides robust predictions of tumour-specific killing across both commercial and primary MPM cell lines.

Recent studies have highlighted the importance of integrating standardised experimental datasets, mechanistic modelling, pharmacokinetic information, and patient-specific biomarkers to advance personalised cell therapy strategies[27,47,48], underlining the need for quantitative tools to support the preclinical evaluation of cellular immunotherapies. Within this context, the proposed framework may serve as a useful starting point for future work aimed at generating virtual patient cohorts and optimising CAR-MET.CIK treatment protocols. Although mathematical and computational models have previously been developed to describe CAR-T cell activity against tumours[21], to our knowledge this is the first study to model tumour antigen expression heterogeneity and predict the antitumour activity of CIK cells.

The results of our work demonstrate that the calibrated model successfully reproduces the experimental data and highlights the positive impact on CAR-MET.CIK killing efficacy of three key variables: the initial CIK-to-tumour cell ratio, the proportion of CIK cells expressing the CAR-MET, and the level of MET expression of the

MPM cell populations. The model performed particularly well in predicting high experimental TSK values, while lower TSK levels were associated with greater variability between numerical and experimental results. While previous works addressing antigen heterogeneity only distinguished between antigen-positive and antigen-negative cells[24], a key strength of the proposed model lies in its ability to integrate the MET expression distribution of the tumour cell population, further capturing intra-tumour heterogeneity, by exploiting clear quantitative markers such as MET% and MFI experimentally accessible via flow cytometry analysis, and make predictions on the expected tumour killing efficacy of CAR-MET.CIK treatment at different CAR% and doses. This may contribute to identifying patient subgroups more likely to benefit from the therapy within clinically attainable E:T ratios. More broadly, the development of predictive modelling approaches such as the one presented here would benefit from increased harmonisation of data collection across *in vitro* studies of cellular immunotherapies. Standardised measurements of tumour antigen expression, effector-cell characteristics, treatment dosing conditions and longitudinal cytotoxicity responses would facilitate model calibration and validation across independent datasets, enabling more robust comparisons between studies and accelerating clinical translation.

The calibrated model points towards cell lines with outlier behaviour that require further analysis, allowing us to identify important biological mechanisms at play when the model performs the worse. This was first the case for the NCI-H2052 cell line (cf. Fig. 3b and Sect. 3.2), for which the model overestimates TSK values. This discrepancy may be explained by the poor/negative expression of NKG2D-specific ligands present on the cell surface, considered to be the main contributor to the cytolysis of CIK cells[11], a feature that was not shared by the other MPM cell lines included in the calibration (see Supp. Mat. Figure S.1). In the absence of NKG2D ligands expressed on the surface of target cells, CIK cytotoxicity is very low as could indeed be observed during model selection, where the reparametrised maximum baseline killing rate $\hat{\gamma}$ for this cell line is notably lower than average – specifically $\hat{\gamma} = 0.045$, at the boundary of the $Q_{2.5\%}$ quantile of the its posterior distribution (cf. Table 4). By using the cell line-specific parameters for the baseline killing function Γ, model predictions of the TSK during NTD.CIK and, consequently, CAR-MET.CIK cytotoxicity assays improves substantially (see Supp. Mat. Figure S.8). Similarly, the calibrated model underestimated the TSK of NTD.CIK G cytotoxicity assays on the MMP primary cell line SL-188 (cf. Fig. 4b, top right panel), the optimal rescaled maximum baseline killing rate $\hat{\gamma}$ of which was found to lie above the $Q_{97.5\%}$ quantile (cf. $\hat{\gamma} = 0.288$ and the $Q_{97.5\%}$ limit value in Table 4) of its posterior distribution. Following the same strategy adopted for the NCI-H2052 cell line, a notable improvement in the TSK fit can be achieved (see Supp. Mat. Figure S.8). These results highlight the ability of our model to accurately capture the killing dynamics. At the same time, they underscore the possibility of strong cell-line specificity of the experimental baseline killing and the presence of additional complexities underlying the cytotoxic mechanisms that are not currently incorporated into the model, thereby preventing an accurate fit for all cell lines. Future extensions of the model to incorporate additional biological factors – such as NKG2D ligand expression levels, which could easily be modelled by an additional phenotypic variable – may improve the model predictive performance.

Translational relevance

The proposed framework establishes a quantitative link between tumour antigen heterogeneity and treatment efficacy through biomarkers that are readily measurable in routine laboratory settings, such as MET positivity and expression intensity. This capability may support biomarker-driven patient stratification and represent an important step towards the development of predictive tools for personalised cellular immunotherapy in MPM cells[21,47]. An additional strength of the framework is that it relies on a limited set of biologically meaningful and experimentally accessible variables. This parsimonious structure may facilitate future clinical implementation, as extensive characterisation of multiple patient-specific biological features is often difficult to achieve in routine clinical practice. Nevertheless, we are aware that a further refinement of the tool is required because our experimental setting does not take into account limitations intrinsic to the solid nature of MPM, related to the ability of CIK to proliferate and persist as active over time, to reach and infiltrate the cancer lesion, to face the hostile tumour microenvironment. The model, now based on short term proliferation data which do not account

for intra- and inter-population competition for space and resources[38], could be improved by updating our growth function model selection and calibration results based on data over a longer timeframe, expected to result in growth functions incorporating saturation effects. Moreover, CAR-CIK cell trafficking from the administration site and tumour infiltration could be further examined, for instance, by coupling the ODE-PIDE model with a pharmacokinetic model describing CAR-T cell administration and distribution[26,49], or implementing an explicit spatial variable for *in situ* infiltration dynamics[50]. Although these developments will surely increase the number of parameters, and may require further calibration of the mathematical framework integrating experimental data obtained from more complex biological models, including *in vitro* tumour organoids and *in vivo* studies, the refinement will more adequately capture the complex spatial dynamics of solid tumours. Such extensions would eventually enable the investigation of long-term therapeutic outcomes, the evaluation of alternative dosing protocols, and the identification of optimal treatment strategies, thus representing a necessary future milestone. Furthermore, the availability of harmonised datasets integrating preclinical cytotoxicity measurements with clinical follow-up information may ultimately allow the investigation of potential associations between model-derived metrics, such as the TSK, and long-term treatment outcomes. Establishing such links would represent an important step towards translating quantitative *in vitro* observations into clinically actionable predictions.

Another crucial point to address in future studies regards the MET-specific killing modulation function $k(x)$, which encodes the influence of tumour MET expression on the cytotoxic activity of CAR-MET.CIK cells. It is the key feature that enables the model, under the same parameter distributions, to reproduce distinct CAR-MET.CIK TSK profiles arising from different initial tumour MET-expression distributions. Its impact becomes evident primarily during the final calibration step, when all MPM cell lines with varying initial MET expression levels are fitted simultaneously. Several other candidate forms of $k(x)$ were explored, and a Hill-type function function was ultimately retained as it provided the best overall agreement with the experimental datasets. Nevertheless, while calibrated model outputs agreed particularly well with experimental data of MPM cell lines with very high MET expression, the model did not perform as well in cell lines with lower MET expression levels. We believe this could be improved with a more targeted and systematic investigation of the function $k(x)$. While initial tests including the Hill function parameters in the calibration procedure highlighted their practical non-identifiability from the available data, optimal control methods are being developed to propose experimental conditions ensuring practical identifiability or model selection in ODE models[51]. Possible future directions include the application of these methods to the ODE-PIDE model presented here, or solving the inverse problem adopting machine learning or deep learning techniques.

From a translational perspective, an accurate characterisation of the relationship between MET density and CAR-mediated cytotoxicity could provide insight into antigen-expression thresholds required for effective tumour control. Such thresholds may ultimately contribute to biomarker-guided patient stratification and help define clinically meaningful criteria for identifying patients more likely to benefit from CAR-MET.CIK therapy. Note that previous theoretical studies of CAR-based therapies did not exclusively focus on the CAR-T therapeutic activity, but covered a range of questions of interest, such as the selection of the best CAR design[52,53], bystander effects[24], cytokine release syndrome onset[54], and immune effector manufacturing optimisation[55]. Nonetheless, the ability of theoretical frameworks to estimate clinically relevant antigen-expression thresholds, and to evaluate their potential impact on treatment efficacy before prospective clinical validation, is increasingly recognised as a critical component of quantitative approaches supporting the clinical development of CAR-based therapies[21,24].

Conclusions

This study demonstrates that experimentally-informed mathematical modelling can accurately capture the interaction between CAR-MET.CIK and MPM cells while explicitly accounting for tumour antigen heterogeneity, thus providing a tool for therapy effectiveness estimation. The modelling framework is inherently flexible and could easily be adapted to different therapeutic targets and tumour types, potentially representing a valuable

predictive tool for treatment efficacy in various oncological contexts. The model supports the broader vision of combining standardised preclinical datasets, mathematical modelling and clinically relevant biomarkers to guide the development of personalised cellular immunotherapies. Future integration of additional immune determinants, pharmacokinetic processes and patient-derived data may further enhance its translational relevance and facilitate the clinical development of CAR-MET.CIK therapy for MPM.

Ultimately, this work illustrates how the integration of experimental immunotherapy data and mechanistic modelling may contribute to the development of more quantitative and personalised approaches for cellular therapies in solid tumours. The broader adoption of harmonised experimental reporting standards, including tumour phenotypic characteristics, effector-cell properties, treatment dosing conditions and longitudinal cytotoxicity measurements, would facilitate model calibration and validation across independent datasets. Such harmonisation may enable more robust comparisons between studies and, when coupled with clinical follow-up information, support the identification of quantitative relationships between preclinical activity and long-term treatment outcomes.

Supplementary Information The online version contains supplementary material available at https://doi.org/10.1038/s41598-026-64219-y.

Acknowledgements We thank Prof. Dario Sangiolo for helpful scientific discussion and Prof. Riccardo Taulli for primary Mesothelioma cell lines.

Author contributions F.P. and A.M.L. equally contributed to this work. E.L. and C.V. share senior authorship. F.P. : Investigation, Methodology, Validation, Formal analysis, Software, Visualization, Writing - original draft. A.M.L. : Investigation, Methodology, Validation, Formal analysis, Visualization, Writing - original draft. S.N. : Writing – review & editing. T.L. : Conceptualization, Supervision, Writing – review & editing. E.V. : Conceptualization, Formal analysis, Supervision, Funding acquisition, Writing – review & editing. E.L. : Conceptualization, Methodology, Formal analysis, Supervision, Writing – review & editing. C.V. : Conceptualization, Methodology, Formal analysis, Supervision, Writing - review & editing.

Funding This research was funded by the University of Torino, grant Ricerca Locale 2022 to E.V.

Data availability All data related to this study are included in this paper and its supplementary information files. No data sets were generated during the current study. Experimental details are available from the corresponding author on reasonable request.

Code availability Padovano, F. & Lombardi, A. M. (2026). Code and data for calibrating and simulating a model of CAR-CIK cell immunotherapy targeting MET-expressing mesothelioma cells (Version v1) [Computer software]. Zenodo. https://doi.org/10.5281/zenodo.21352734.

Declarations

Competing interests The authors declare no competing interests.

Open Access This article is licensed under a Creative Commons Attribution-NonCommercial-NoDerivatives 4.0 International License, which permits any non-commercial use, sharing, distribution and reproduction in any medium or format, as long as you give appropriate credit to the original author(s) and the source, provide a link to the Creative Commons licence, and indicate if you modified the licensed material. You do not have permission under this licence to share adapted material derived from this article or parts of it. The images or other third party material in this article are included in the article's Creative Commons licence, unless indicated otherwise in a credit line to the material. If material is not included in the article's Creative Commons licence and your intended use is not permitted by statutory regulation or exceeds the permitted use, you will need to obtain permission directly from the copyright holder. To view a copy of this licence, visit http://creativecommons.org/licenses/by-nc-nd/4.0/.

References

1. Blattman, J. N. & Greenberg, P. D. Cancer immunotherapy: A treatment for the masses. *Science* **305**(5681), 200–205 (2004).
2. Wang, Z. & Cao, Y. J. Adoptive cell therapy targeting neoantigens: a frontier for cancer research. *Front. Immunol.* **11**, 176 (2020).
3. Albarrán, V., San Román, M., Pozas, J., Chamorro, J., Rosero, D.I., Guerrero, P., Calvo, J.C., Gonzalez, C., García de Quevedo, C., Pérez de Aguado, P. et al. Adoptive T cell therapy for solid tumors: current landscape and future challenges, *Front. Immunol.* **15**, 1352805 (2024).
4. Morotti, M. et al. Promises and challenges of adoptive T-cell therapies for solid tumours. *Br. J. Cancer* **124**(11), 1759–1776 (2021).
5. Jayaraman, J. et al. CAR-T design: Elements and their synergistic function. *EBioMedicine* 58 (2020).
6. Abbasi, S. et al. Chimeric antigen receptor T (CAR-T) cells: Novel cell therapy for hematological malignancies. *Cancer Med.* **12**(7), 7844–7858 (2023).
7. Rafii, S. et al. Advancing CAR T-cell therapy in solid tumors: current landscape and future directions. *Cancers* **17**(17), 2898 (2025).
8. Chen, T., Wang, M., Chen, Y. & Liu, Y. Current challenges and therapeutic advances of CAR-T cell therapy for solid tumors. *Cancer Cell Int.* **24**(1), 133 (2024).
9. Fennell, D. A., Dulloo, S. & Harber, J. Immunotherapy approaches for malignant pleural mesothelioma. *Nat. Rev. Clin. Oncol.* **19**(9), 573–584 (2022).
10. Scherpereel, A., Wallyn, F., Albelda, S. M. & Munck, C. Novel therapies for malignant pleural mesothelioma. *Lancet Oncol.* **19**(3), e161–e172 (2018).
11. Mesiano, G. et al. Cytokine-induced killer (CIK) cells as feasible and effective adoptive immunotherapy for the treatment of solid tumors. *Expert Opin. Biol. Ther.* **12**(6), 673–684 (2012).
12. Lombardi, A. M., Sangiolo, D. & Vigna, E. MET oncogene targeting for cancer immunotherapy. *Int. J. Mol. Sci.* **25**(11), 6109 (2024).
13. Santoni-Rugiu, E. et al. Correlation of MET-Receptor Overexpression with MET Gene Amplification and Patient Outcome in Malignant Mesothelioma. *Int. J. Mol. Sci.* **22**(23), 12868 (2021).
14. Altrock, P. M., Liu, L. L. & Michor, F. The mathematics of cancer: integrating quantitative models. *Nat. Rev. Cancer* **15**(12), 730–745 (2015).
15. De Pillis, L.G., Radunskaya, A.E. & Wiseman, C.L. A validated mathematical model of cell-mediated immune response to tumor growth, *Cancer Res.* (2005).
16. Eftimie, R., Bramson, J. L. & Earn, D. J. Interactions between the immune system and cancer: a brief review of non-spatial mathematical models. *Bull. Math. Biol.* **73**(1), 2–32 (2011).
17. Mahlbacher, G. E., Reihmer, K. C. & Frieboes, H. B. Mathematical modeling of tumor-immune cell interactions. *J. Theor. Biol.* **469**, 47–60 (2019).
18. Wilkie, K.P. A review of mathematical models of cancer–immune interactions in the context of tumor dormancy. *Syst. Biol. Tumor Dormancy* 201–234, (2012).
19. Kimmel, G.J., Locke, F.L. & Altrock, P.M. Response to CAR T cell therapy can be explained by ecological cell dynamics and stochastic extinction events. *bioRxiv*, p. 717074, (2019).
20. Kirouac, D. C. et al. Deconvolution of clinical variance in CAR-T cell pharmacology and response. *Nat. Biotechnol.* **41**(11), 1606–1617 (2023).
21. Putignano, G., Ruipérez-Campillo, S., Yuan, Z., Millet, J. & Guerrero-Aspizua, S. Mathematical models and computational approaches in CAR-T therapeutics. *Front. Immunol.* **16**, 1581210 (2025).
22. Sabir, S., León-Triana, O., Serrano, S., Barrio, R. & Pérez-García, V. M. Mathematical model of CAR T-cell therapy for a B-cell lymphoma lymph node. *Bull. Math. Biol.* **87**(3), 40 (2025).
23. Sinelshchikov, D., Belmonte-Beitia, J. & Italia, M. A mathematical model of CAR-T cell therapy in combination with chemotherapy for malignant gliomas. *Chaos Interdiscip. J. Nonlinear Sci.* **35**(6) (2025).
24. Kara, E., Jackson, T.L., Jones, C., Sison, R. & McGee Ii, R.L. Mathematical modeling insights into improving CAR T cell therapy for solid tumors with bystander effects. *NPJ Syst. Biol. Appl.* **10**(1), 105 (2024).
25. Luque, L. M., Carlevaro, C. M., Rodriguez-Lomba, E. & Lomba, E. In silico study of heterogeneous tumour-derived organoid response to CAR T-cell therapy. *Sci. Rep.* **14**(1), 12307 (2024).
26. Singh, A.P., Zheng, X., Lin-Schmidt, X., Chen, W., Carpenter, T.J., Zong, A., Wang, W. & Heald, D.L. Development of a quantitative relationship between CAR-affinity, antigen abundance, tumor cell depletion and CAR-T cell expansion using a multiscale systems PK-PD model, in *MAbs*, vol. 12, p. 1688616, Taylor & Francis, (2020).
27. Barros, L. R. et al. CART math-a mathematical model of CAR-T immunotherapy in preclinical studies of hematological cancers. *Cancers* **13**(12), 2941 (2021).
28. Almeida, L., Audebert, C., Leschiera, E. & Lorenzi, T. Discrete and continuum models for the coevolutionary dynamics between CD8+ cytotoxic T lymphocytes and tumour cells. *Math. Med. Biol. J. IMA* **40**(2), 141–174 (2023).

29. Chisholm, R. H., Lorenzi, T., Desvillettes, L. & Hughes, B. D. Evolutionary dynamics of phenotype-structured populations: from individual-level mechanisms to population-level consequences. *Z. Angew. Math. Phys.* **67**(4), 100 (2016).
30. Lorenzi, T., Chisholm, R. H. & Clairambault, J. Tracking the evolution of cancer cell populations through the mathematical lens of phenotype-structured equations. *Biol. Direct* **11**(1), 43 (2016).
31. Almeida, L. et al. Evolutionary dynamics of glucose-deprived cancer cells: insights from experimentally informed mathematical modelling. *J. R. Soc. Interface* **21**(210), 20230587 (2024).
32. Browning, A. P. et al. Identifiability of phenotypic adaptation from low-cell-count experiments and a stochastic model. *PLoS Comput. Biol.* **21**(6), e1013202 (2025).
33. Sahoo, P., Yang, X., Abler, D., Maestrini, D., Adhikarla, V., Frankhouser, D., Cho, H., Machuca, V., Wang, D., Barish, M. et al. Mathematical deconvolution of CAR T-cell proliferation and exhaustion from real-time killing assay data, *J. R. Soc. Interface* **17**(162) (2020).
34. Motulsky, H. & Christopoulos, A. Fitting models to biological data using linear and nonlinear regression: a practical guide to curve fitting (Oxford University Press, 2004).
35. Anobile, D. P. et al. Evaluation of the preclinical efficacy of Lurbinectedin in malignant pleural mesothelioma. *Cancers* **13**(10), 2332 (2021).
36. Chiriaco, C. et al. Efficacy of CAR-T immunotherapy in MET overexpressing tumors not eligible for anti-MET targeted therapy. *J. Exp. Clin. Cancer Res.* **41**(1), 309 (2022).
37. Leuci, V. et al. CSPG4-specific CAR. CIK lymphocytes as a novel therapy for the treatment of multiple soft-tissue sarcoma histotypes. *Clin. Cancer Res.* **26**(23), 6321–6334 (2020).
38. Benzekry, S. et al. Classical mathematical models for description and prediction of experimental tumor growth. *PLoS Comput. Biol.* **10**(8), e1003800 (2014).
39. Weiss, J. N. The Hill equation revisited: uses and misuses. *FASEB J.* **11**(11), 835–841 (1997).
40. Celora, G. L. et al. A DNA-structured mathematical model of cell-cycle progression in cyclic hypoxia. *J. Theor. Biol.* **545**, 111104 (2022).
41. Spilker, M. E. & Vicini, P. An evaluation of extended vs weighted least squares for parameter estimation in physiological modeling. *J. Biomed. Inform.* **34**(5), 348–364 (2001).
42. The MathWorks, Inc., *Optimization Toolbox, version 2024b*. The MathWorks, Inc., Natick, Massachusetts, 2024. MATLAB Optimization Toolbox. Available from: https://www.mathworks.com/products/optimization.html.
43. Banks, H. & Joyner, M. L. AIC under the framework of least squares estimation. *Appl. Math. Lett.* **74**, 33–45 (2017).
44. Linden, N. J., Kramer, B. & Rangamani, P. Bayesian parameter estimation for dynamical models in systems biology. *PLoS Comput. Biol.* **18**(10), e1010651 (2022).
45. Valderrama-Bahamóndez, G. I. & Fröhlich, H. MCMC techniques for parameter estimation of ODE based models in systems biology. *Front. Appl. Math. Stat.* **5**, 55 (2019).
46. Clerx, M. et al. Probabilistic inference on Noisy Time Series (PINTS). *J. Open Res. Softw.* **7**(1), 23 (2019).
47. Murias-Closas, A., Prats, C., Calvo, G., López-Codina, D. & Olesti, E. Computational modelling of car t-cell therapy: from cellular kinetics to patient-level predictions. *EBioMedicine* 113 (2025).
48. Qi, T., McGrath, K., Ranganathan, R., Dotti, G. & Cao, Y. Cellular kinetics: A clinical and computational review of car-t cell pharmacology. *Adv. Drug Deliv. Rev.* **188**, 114421 (2022).
49. Padovano, F. & Villa, C. The development of drug resistance in metastatic tumours under chemotherapy: an evolutionary perspective. *J. Theor. Biol.* **595**, 111957 (2024).
50. Almeida, L., Audebert, C., Leschiera, E. & Lorenzi, T. A hybrid discrete-continuum modelling approach to explore the impact of t-cell infiltration on anti-tumour immune response. *Bull. Math. Biol.* **84**(12), 141 (2022).
51. Liu, Y., Maini, P. K. & Baker, R. E. Optimal experiment design for practical parameter identifiability and model discrimination. *Math. Biosci.* **399**, 109710 (2026).
52. Tserunyan, V. & Finley, S. D. Computational analysis of 4–1bb-induced nfκb signaling suggests improvements to car cell design. *Cell Commun. Signal.* **20**(1), 129 (2022).
53. Santurio, D. S. & Barros, L. R. C. A mathematical model for on-target off-tumor effect of car-t cells on gliomas. *Front. Syst. Biol.* **2**, 923085 (2022).
54. Zhang, Z., Liu, L., Ma, C. & Chen, W. A computational model of cytokine release syndrome during car t-cell therapy. *Adv. Ther.* **5**(10), 2200130 (2022).
55. Colina, A. S. et al. Current advances in experimental and computational approaches to enhance car t cell manufacturing protocols and improve clinical efficacy. *Front. Mol. Med.* **4**, 1310002 (2024).

Publisher's note Springer Nature remains neutral with regard to jurisdictional claims in published maps and institutional affiliations.

Authors and Affiliations

Federica Padovano[1] · Andrea Maria Lombardi[2] · Silvia Novello[2] · Tommaso Lorenzi[3] · Elisa Vigna[2] · Emma Leschiera[4] · Chiara Villa[5]

✉ Chiara Villa
chiara.villa@math.cnrs.fr

1 Laboratoire Jacques-Louis Lions, Sorbonne Université, CNRS, Université de Paris, Paris, France

2 Laboratory of Translational Oncology P. Gilardi, Department of Oncology, University of Torino, Orbassano, Italy

3 Dipartimento di Scienze Matematiche, Politecnico di Torino, Torino, Italy

4 De Vinci Higher Education, De Vinci Research Center, Paris, France

5 MAP5, Université Paris Cité, CNRS, Paris, France